
TRAINING FREE GRAPH NEURAL NETWORKS FOR GRAPH MATCHING

A PREPRINT

Zhiyuan Liu*
acharkq@gmail.com

Yixin Cao†
caoyixin2011@gmail.com

Fuli Feng*
fulifeng93@gmail.com

Xiang Wang*
xiangwang@u.nus.edu

Jie Tang‡
jietang@tsinghua.edu.cn

Kenji Kawaguchi*
kenji@comp.nus.edu.sg

Tat-Seng Chua*
chuats@comp.nus.edu.sg

ABSTRACT

We present a framework of **Training Free Graph Matching (TFGM)** to boost the performance of Graph Neural Networks (GNNs) based graph matching, providing a fast promising solution without training (training-free). TFGM provides four widely applicable principles for designing training-free GNNs and is generalizable to supervised, semi-supervised, and unsupervised graph matching. The keys are to handcraft the matching priors, which used to be learned by training, into GNN’s architecture and discard the components inessential under the training-free setting. Further analysis shows that TFGM is a linear relaxation to the quadratic assignment formulation of graph matching and generalizes TFGM to a broad set of GNNs. Extensive experiments show that *GNNs with TFGM* achieve comparable (if not better) performances to their fully trained counterparts, and demonstrate TFGM’s superiority in the unsupervised setting. Our code is available at <https://github.com/acharkq/Training-Free-Graph-Matching>.

1 Introduction

Graph matching aims to find equivalent nodes between graphs while respecting the compatibility of node features and graph structures (Wang et al., 2019a). It is crucial in many real-world applications, such as to match keypoints on images (Zanfir and Sminchisescu, 2018), find equivalent entities between knowledge graphs (KGs) (Sun et al., 2017), and link users across different social networks (Zhang et al., 2019a). To better abstract node features for matching, it has become a *de facto* standard to train GNNs in supervised or semi-supervised models (Fey et al., 2020; Sun et al., 2020). There are two key difficulties in the training process. On one hand, graph matching’s annotation is often limited (Berrendorf et al., 2021) and sometimes unavailable (Saraph and Milenković, 2014). This is because graph matching’s annotation is generally labor-intensive due to the large candidate space (Zhong et al., 2018). In specific domains, annotation is further barriered by issues like cross-language (*e.g.*, KGs (Chen et al., 2016)), incomplete profile (*e.g.*, social networks (Zhong et al., 2018)) or lacking expertise knowledge (*e.g.*, protein networks (Ficklin and Feltus, 2011)). On the other hand, training GNNs is computationally expensive due to the exponentially growing number of neighbors with depth (Chiang et al., 2019; Zou et al., 2019).

These difficulties accompanied with training raise the following **Research Questions**. **RQ1**: Is it possible to conduct graph matching using GNNs without training? **RQ2**: To what extent, can we apply such training-free setting in real applications? **RQ3**: What are the differences when designing training-free neural architectures? To resolve these questions, we present the **Training Free Graph Matching (TFGM)** framework for graph matching with GNNs without training. We propose and justify four principles to design training-free GNNs that are generalizable to supervised, semi-supervised, and unsupervised graph matchings.

*School of Computing, National University of Singapore

†School of Computing, Singapore Management University

‡Computer Science Department, Tsinghua University

Table 1: Results on graph matching benchmark DBPZH-EN (Sun et al., 2017). GNNs share the same architecture (except residual connection), but differ in the weights.

Model	Accuracy (%)
NodeMatch	60.3
Training-free GNN w/o residual	37.2
Training-free GNN w residual	62.5
Fully trained GNN	70.4

RQ1. We show that TFGM is a linear assignment problem (LAP) relaxation of graph matching’s quadratic assignment problem (QAP) formulation (Caetano et al., 2009; Cho et al., 2013), which can preserve both node compatibility and structural compatibility. The preliminary results in Table 1 demonstrate our analysis: a training-free GNN outperforms NodeMatch, which directly compares node features without any structural information. As expected, training-free GNNs perform worse than the fully trained GNN, posing a great challenge of incorporating knowledge that trained models can learn into the training-free framework.

RQ2. We generalize the unsupervised TFGM to supervised, semi-supervised settings by incorporating annotations without training. Annotation contains crucial knowledge of matching. We let training-free GNNs use annotation to match fully trained GNNs’ performance. The general principle is to leverage annotation to generate more discriminative node representation: for the supervised graph matching, we design a label-discriminative feature to mine potential alignment signals from annotation data via kNN search; for the semi-supervised graph matching, we propose a node feature initialization strategy to incorporate alignment signal.

RQ3. We propose two rules of training-free neural architectures, inspiring four design Principles for GNNs. 1) Handcraft matching priors, which used to be learned by training, into GNN architecture. The first rule explains that powerful architecture leads to better performance (**P4**). It also implies using annotation (**P2**). We further let node embedding to preserve neighbors of different localities (**P1**) to enable a strict matching of neighbors in the same order. 2) Discard the components inessential for training-free. We remove the nonlinearity between layers and propose weight-free GNN to eliminate the noise caused by random weights (**P3**).

For evaluation, we extensively experiment on three benchmarks, including (supervised) Keypoint Matching (Zanfir and Sminchisescu, 2018), (semi-supervised) Entity Alignment (Sun et al., 2017), and (unsupervised) Protein-Protein Interaction Network Alignment (Vijayan et al., 2015). We test TFGM with GraphSAGE (Hamilton et al., 2017), SplineCNN (Fey et al., 2018), and DGMC (Fey et al., 2020). Experimental results support our analysis and demonstrate the effectiveness of TFGM. TFGM achieves significant improvements than unsupervised models and performs comparable (if not better) to fully trained GNNs in supervised and semi-supervised settings. Ablation studies verify TFGM’s main components and the efficient training-free property.

2 Related Work

2.1 Graph Matching

Technical Route. Graph matching is mathematically formulated as an NP-hard QAP. Thus, initial works focus on relaxation to deal with the intractability (Conte et al., 2004). In practice, graph matching can be eased by comparing graph attributes. To better measure the similarity of attributes, SVM, CNN, and GNN are successively introduced for graph matching (Caetano et al., 2009; Zanfir and Sminchisescu, 2018; Wang et al., 2019a; Xu et al., 2019). Initially, deep learning methods are introduced to obtain better feature representations. A natural idea for improvement is thus to embed existing combinatorial solvers into neural networks (Wang et al., 2019a; Sarlin et al., 2020). This idea has been applied on graph matching’s LAP relaxation by applying the differentiable Sinkhorn networks (Cuturi, 2013; Mena et al., 2017). Rolínek et al. (2020) further combine GNNs with an advanced QAP solver based on Lagrange decomposition (Swoboda et al., 2017; 2019) for graph matching. Meanwhile, GNNs are also studied as combinatorial solvers instead of feature extractors (Wang et al., 2019b; Fey et al., 2020). Our work shares similar spirits. We show that GNNs can be used to relax the QAP to make the problem tractable. More importantly, we show that GNN’s fitness to graph matching is independent of training.

Applications. Graph matching has various applications, including social networks, KGs, and Computer Vision (CV). Social networks are large graphs with rich topological patterns. Graph matching models rely on the *isomorphic assumption* and aim to maximize the structural consistency (Zhang and Philip, 2015; Zhang et al., 2019a). We can leverage attributes (Yan et al., 2021) and additional networks (Chu et al., 2019) for improvement. Similarly, Entity Alignment combines structures and attributes to find equivalent entities between KGs. Knowledge graph embedding models and relation-aware GNNs are adopted to learn the heterogeneous graphs (Sun et al., 2020; Zhao et al., 2020).

In CV, graph matching is applied to find the semantic equivalent keypoints between different objects (Zanfir and Sminchisescu, 2018) and the same object’s points but from different perspectives (Sarlin et al., 2020). Geometric prior is studied to benefit object tracking (Chen et al., 2001), pose estimation (Girdhar et al., 2018), and point cloud registration (Wang and Solomon, 2019). In these applications, training has been a long-standing issue due to the limited annotation (Chen et al., 2016; Zhou et al., 2021) and scalability (Zhu et al., 2020; Mao et al., 2021). Thus, we seek solutions from training-free strategies.

2.2 Training-free Neural Networks

Graph-Augmented MLPs. TFGM is related to Graph-Augmented MLPs (GA-MLPs) (Chen et al., 2019; Wu et al., 2019). GA-MLPs obtain structure-aware node embeddings by applying a set of graph operators on node features. This step is training-free because graph operators are dependent only on structure, *e.g.*, the adjacency matrix. Further, GA-MLPs train a classifier on top of structure-aware node embeddings for downstream tasks and have achieved very competitive performance to full GNNs. Because the training is independent of graph structure, GA-MLPs are trivially scalable to large graphs (Frasca et al., 2020). The idea is firstly introduced in SGC (Wu et al., 2019), which uses the power of a normalized adjacency matrix as the graph operator. The graph operator is demonstrated to be a low-pass filter (Wu et al., 2019; Nt and Maehara, 2019). Frasca et al. (2020) enlarge the family of graph operators. Chen et al. (2021) theoretically show that the VC-dimension of existing GA-MLPs grows poly-exponentially with the number of layers. Zambon et al. (2020) show that graph distance defined by training-free GNNs is metric. TFGM is different from previous works in that we focus on graph matching, which requires solving a combinatorial optimization problem.

Neural Networks with Random Weights. TFGM is ideally similar to the Neural Networks with Random Weights (NNRW), which initiates from Random Vector Functional Link networks (Igel and Pao, 1995). It is proved that NNRW, in which weights between the input and hidden layers are randomly assigned, are universal approximators (Li et al., 1997; Huang et al., 2006). The works on CNNs with random filters further expand NNRW to practical applications of object detection and image restoration (Jarrett et al., 2009; Saxe et al., 2011; Ulyanov et al., 2018). These works demonstrate that NNRW can be used to obtain meaningful representation that is linearly separable for downstream tasks. Inspired by previous works, we propose TFGM to obtain graph representation with training-free GNNs.

3 Methodology

In this section, we introduce TFGM for the unsupervised graph matching, followed by TFGMws that generalizes TFGM to supervised and semi-supervised graph matching.

3.1 Problem Formulation

We define a graph as $\mathcal{G} = (\mathcal{V}, A, X, E)$, where $\mathcal{V} = \{1, 2, \dots\}$ is the set of nodes, $A \in \{0, 1\}^{|\mathcal{V}| \times |\mathcal{V}|}$ is the adjacency matrix, $X \in \mathbb{R}^{|\mathcal{V}| \times d_x}$ is the node feature, and $E \in \mathbb{R}^{|\mathcal{V}|^2 \times d_e}$ is the edge feature. d_x and d_e are the dimension sizes for features of nodes and edges. Given graphs $\mathcal{G}^{(s)} = (\mathcal{V}^{(s)}, A^{(s)}, X^{(s)}, E^{(s)})$ and $\mathcal{G}^{(t)} = (\mathcal{V}^{(t)}, A^{(t)}, X^{(t)}, E^{(t)})$, *w.l.o.g.*, let $|\mathcal{V}^{(s)}| \leq |\mathcal{V}^{(t)}|$, graph matching (Caetano et al., 2009; Cho et al., 2013) can be formulated as a QAP:

$$S^* = \operatorname{argmax}_{S \in \mathcal{T}} \sum_{\substack{i \in \mathcal{V}^{(s)} \\ j \in \mathcal{V}^{(t)}}} Q_{ij} S_{ij} + \sum_{\substack{i, i' \in \mathcal{V}^{(s)} \\ j, j' \in \mathcal{V}^{(t)}}} T_{ii'; jj'} S_{ij} S_{i'j'}, \quad (1)$$

where $S \in \{0, 1\}^{|\mathcal{V}^{(s)}| \times |\mathcal{V}^{(t)}|}$ is an assignment matrix such that $S_{ij} = 1$ iff $i \in \mathcal{V}^{(s)}$ is mapped to $j \in \mathcal{V}^{(t)}$. The entry Q_{ij} of the matrix $Q \in \mathbb{R}^{|\mathcal{V}^{(s)}| \times |\mathcal{V}^{(t)}|}$ measures nodes’ similarity based on their features $X_i^{(s)}$ and $X_j^{(t)}$. $T_{ii'; jj'}$ measures similarity between edge features $E_{(i, i')}^{(s)}$ and $E_{(j, j')}^{(t)}$. The set $\mathcal{T} = \{S \in \{0, 1\}^{|\mathcal{V}^{(s)}| \times |\mathcal{V}^{(t)}|} : [\forall j \in \mathcal{V}^{(t)}, \sum_{i \in \mathcal{V}^{(s)}} S_{ij} \leq 1] \wedge [\forall i \in \mathcal{V}^{(s)}, \sum_{j \in \mathcal{V}^{(t)}} S_{ij} = 1]\}$ represents the assignment constraints to guarantee a one-to-one mapping. In Equation (1), the first linear term is to preserve the compatibility between nodes; the second quadratic term is to preserve the compatibility between edges.

If not noted, we apply the GCN-flavored definition of GNNs:

$$l = 0 : \quad \text{GNN}_l(A, X) = H^{(l)} = X, \quad (2)$$

$$l = 1, \dots, L : \quad \begin{cases} \text{GNN}_l(A, X) = AH^{(l-1)}W_l, \\ H^{(l)} = \sigma(\text{GNN}_l(A, X)), \end{cases} \quad (3)$$

where σ is a nonlinear activation function. $\{W_l\}_1^L$ is a series of trainable matrices. If the GNN is training-free, all matrices in $\{W_l\}_1^L$ are randomly sampled from $\frac{1}{\sqrt{d}}\mathcal{N}(\mathbf{0}, \mathbf{I})$. d is the dimension of the hidden layer. This definition can be easily generalized to existing GNNs (Kipf and Welling, 2017; Hamilton et al., 2017) by replacing the adjacency matrix A with the corresponding graph operators.

3.2 Training Free Graph Matching

Like other machine learning methods, graph matching with GNNs has two phases: training and inference. In the training phase, the weights in GNNs are optimized to pull the embeddings of equivalent nodes together and push different nodes away. In the inference stage, we compute the similarities between node embeddings generated by the fully trained GNNs for graph matching. In light of the preliminary studies (Chen et al., 2021) and experiments (Table 1), we hypothesize that the weights in GNNs are not crucial for graph matching, but the majority comes from the inductive bias in GNN’s architecture. We, therefore, propose the BasicTFGM that skips the training phase and directly applies randomly initialized GNNs for graph matching inference.

Definition 1 (BasicTFGM). Given an arbitrary training-free graph neural network $\phi : \mathcal{G} \mapsto \phi(\mathcal{G}) \in \mathbb{R}^{|\mathcal{V}| \times d}$, *BasicTFGM* with ϕ is defined by finding the assignment S^* that maximizes the dot-product of corresponding nodes’ embeddings:

$$S^* = \operatorname{argmax}_{S \in \mathcal{T}} \sum_{i \in \mathcal{V}^{(s)}, j \in \mathcal{V}^{(t)}} S_{ij} \left(\phi(\mathcal{G}^{(s)}) \phi(\mathcal{G}^{(t)})^\top \right)_{ij}. \quad (4)$$

From Table 1, we observe that training free GNN’s performance drops by 25% if residual connection is disabled, showing the importance of lower-order information. The BasicTFGM only measures the similarities between nodes concerning their L -th order neighborhoods. The lower-order information may be crucial but “washed out” during feedforward. We, therefore, propose TFGM for improvement.

Definition 2 (TFGM). For an arbitrary L -layer graph neural network ϕ_L , let $\phi_l (0 \leq l \leq L)$ be the first l layers of ϕ_L . *TFGM* with ϕ_L is defined by finding the assignment matrix S^* that maximizes the cosine similarity of corresponding node embeddings from all GNN layers as:

$$S^* = \operatorname{argmax}_{S \in \mathcal{T}} \sum_{i \in \mathcal{V}^{(s)}, j \in \mathcal{V}^{(t)}} S_{ij} \left(\sum_{l=0}^L \operatorname{Cos} \left(\phi_l(\mathcal{G}^{(s)}), \phi_l(\mathcal{G}^{(t)}) \right) \right)_{ij}. \quad (5)$$

TFGM enhances the BasicTFGM by preserving different orders of neighbor information and also the initial node feature ($l = 0$) to facilitate a comprehensive similarity measurement. Further, because the norms of graph embeddings can change over different layers, we normalize the node embeddings at every layer by replacing dot-product with cosine similarity. TFGM guarantees the strict matching of neighbors from the same order and enforces the prior that information of different orders should weigh the same. The similarity measurements of different orders are summarized into a single linear term, guaranteeing to be solvable within polynomial time. Compared to the BasicTFGM, TFGM is more robust to over-smoothing because it considers the neighborhoods of all $0, 1, \dots, L$ orders, wherein the over-smoothing issue usually happens in high-order layers that cannot affect the comparisons of low-order layers.

3.3 Utilizing Annotation without Training

So far, TFGM can well suit the unsupervised graph matching. We now generalize TFGM to the supervised and semi-supervised settings. The annotation data can supervise graph matching models to perform better feature extraction (Cho et al., 2013) and support the matching of uncertain nodes with close-by ground truth matchings (Rocco et al., 2018). To this end, we introduce two strategies for TFGM to utilize such priors without training. The enhanced TFGM is termed as TFGMws (TFGM with supervision).

The general principle of both strategies is to leverage annotation to generate more discriminative node representations. We present the core ideas of the strategies. Detailed algorithms are in Appendix D. Given two graphs $\mathcal{G}^{(s)}$ and $\mathcal{G}^{(t)}$, both settings aim to find an assignment S^* that corresponds to the equivalent mapping between $\mathcal{V}^{(s)}$ and $\mathcal{V}^{(t)}$.

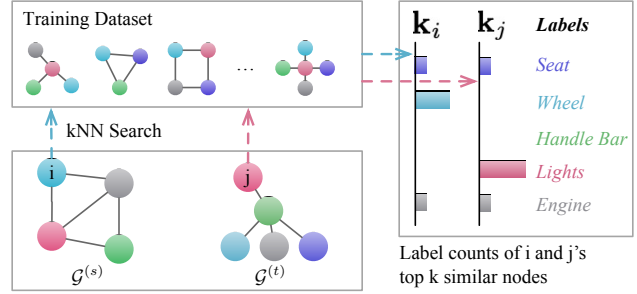
Supervised Graph Matching provides node labels for graphs in a training set \mathcal{D} (Bourdev and Malik, 2009; Everingham et al., 2010; Cho et al., 2013). Unlike node classification, the node labels are mutually exclusive within one graph. For graph matching, nodes with the same label but from different graphs are marked as equivalent.

To utilize annotation without training, we generate a label-discriminative feature \mathbf{k}_i for all node i in $\mathcal{G}^{(s)}$ and $\mathcal{G}^{(t)}$ by performing a kNN search in training dataset (Figure 1a). The basic idea is to find i ’s k closest nodes in training dataset

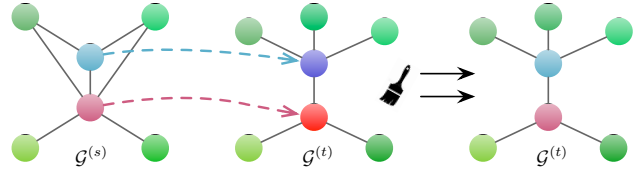
and use the labels of these k nodes as \mathbf{k}_i . If i is a *wheel* of a motorbike, \mathbf{k}_i will have a high *wheel* score. \mathbf{k}_i captures the priors in annotation and is more discriminative than the node’s original feature. Thus, we solve the LAP with node similarity measured by $\text{Cos}(\mathbf{k}_i, \mathbf{k}_j)$ ($\forall i \in \mathcal{V}^{(s)}, j \in \mathcal{V}^{(t)}$).

We present the steps to generate \mathbf{k}_i for node i in an arbitrary graph \mathcal{G} . The strategy is a variant of Matching Networks (Vinyals et al., 2016). 1) We conduct graph matching between \mathcal{G} and every graph in the training dataset \mathcal{D} using the unsupervised TFGM, and thus obtain the similarity scores between i and every node in the training dataset. 2) For each graph in the training dataset, we keep only the most similar node to i . 3) Select the top k nodes $\mathcal{L} = \{v_1, v_2, \dots, v_k\}$ that have the largest similarity scores to i . 4) Let $\mathbf{k}_i = \sum_{v \in \mathcal{L}} \mathbf{y}_v$, where \mathbf{y}_v is the one-hot encoding of node v ’s label.

Semi-supervised Graph Matching provides a set of annotated equivalent node pairs $\mathcal{I} = \{(i, j) | i \in \mathcal{V}^{(s)}, j \in \mathcal{V}^{(t)}\}$ as supervision. The goal is to find equivalent nodes among the unannotated nodes in $\mathcal{G}^{(s)}$ and $\mathcal{G}^{(t)}$. To incorporate annotation, we set the initial features of nodes in \mathcal{I} to be the same (Figure 1b): for all $(i, j) \in \mathcal{I}$, let $X_i^{(s)} \rightarrow X_j^{(t)}$ or vice versa. The intuition is that GNNs can propagate the strong equivalence signal, *i.e.*, $\text{Cos}(X_i^{(s)}, X_j^{(t)}) = 1$, to neighbors of i and j , and thus support their matching. This strategy operates on the feature initialization phase and adds $O(|\mathcal{I}|d)$ computation overhead, which is much cheaper than training.



(a) Supervised setting. Generate node i and j ’s label-discriminative feature \mathbf{k}_i and \mathbf{k}_j with kNN search. Different colors denote different node labels. Example labels are from a motorbike.



(b) Semi-supervised setting. Force known equivalent nodes (connected by dashed arrows) to have the same initial node features.

Figure 1: Diagrams for utilizing annotation without training.

4 Design Principles and Justification

4.1 Design Principles of TFGM

We summarize our framework as four design Principles to boost the performance of training-free GNNs for graph matching. They enable training-free GNNs to perform comparably to their fully trained counterparts.

- **P1**: Concatenate the normalized embeddings from all GNN layers as node representations (Section 3.2);
- **P2**: If annotation is available, use it to generate more discriminative node representations (Section 3.3);
- **P3**: For GCN-flavored GNNs, *e.g.*, $\text{GNN}_l(A, X) = AH^{(l-1)}W_l$, where A is a graph operator. Use their weight-free versions, *e.g.*, $\text{GNN}_l(A, X) = AH^{(l-1)}$;
- **P4**: Explore more powerful graph operators/kernels.

P1 and **P2** are intuitively explained in previous section. **P3** is to eliminate the random noise caused by random weights. **P4** encourages the exploration of more appropriate inductive bias for the dataset. Pioneer study (Saxe et al., 2011) and our experiments show that better architecture leads to better performance even in the training-free setting.

In the rest of this section, we justify TFGM by showing that it is a linear relaxation of graph matching’s QAP formulation. Further, we show that random-weight GNN is an unbiased estimator of weight-free GNN for graph matching if nonlinearity is removed (**P3**). Finally, we generalize TFGM to more GNNs (**P4**).

4.2 TFGM is a Linear Relaxation of the QAP

As stated in Equation (1), graph matching is a QAP, which is NP-hard. We now show that *BasicTFGM with GNN* is a linear relaxation of the QAP. Inspired by the neighborhood consensus (Rocco et al., 2018; Fey et al., 2020), we relax the quadratic term in Equation (1) to linear as follows:

$$S^* = \underset{S \in \mathcal{T}}{\text{argmax}} \sum_{\substack{i \in \mathcal{V}^{(s)} \\ j \in \mathcal{V}^{(t)}}} Q_{ij} S_{ij} + \sum_{\substack{i, i' \in \mathcal{V}^{(s)} \\ j, j' \in \mathcal{V}^{(t)}}} A_{ii'}^{(s)} A_{jj'}^{(t)} P_{i'j'}^{(ij)} S_{ij}, \quad (6)$$

where $T_{i'i',j'j'}$ is measured by $A_{i'i'}^{(s)}A_{j'j'}^{(t)}$, a binary indicator for the existence of edges (i, i') and (j, j') ; one of the assignment $S_{i'j'}$ is replaced by its approximate estimation $P_{i'j'}^{(ij)} \in \mathbb{R}^{(|\mathcal{V}^{(s)}| \times |\mathcal{V}^{(t)}|)^2}$, which is a 4-dimensional tensor. We give P a superscript (ij) (i.e., two extra dimensions) to maintain $S_{i'j'}$'s dependence on index (ij) – because $S_{i'j'}$ is an optimization variable, its value is dependent on the other optimization variable S_{ij} . In other words, this superscript allows P to measure the similarity between i' and j' while considering the matching of other nodes. To summarize, Equation (6) holds a similar objective to Equation (1) – find an assignment matrix S^* that maximizes the node compatibility and structural compatibility.

Note that, Equation (6) becomes an LAP, if Q and P have no weights to be optimized. Thus, we can solve it within polynomial time with a theoretical guarantee. Now, the core problem is to find suitable functions that can produce a good estimation of Q and P . However, is it feasible to find good compatibility measurements Q and P that 1) require no training and 2) can measure equivalence between nodes and structures? The answer is yes. Let us first focus on the node compatibility measurement Q . When nodes have real-world features, such as text names and image patches, thanks to the development of pre-trained models, non-parametric functions (e.g., dot-product and cosine similarity) based on embeddings of the real-world features can largely measure the semantic equivalence (Reimers and Gurevych, 2019).

Next, we move forward to the structural compatibility P by applying the *BasicTFGM with GNN*.

Proposition 1. *BasicTFGM with $\text{GNN}_L(A, X)$ is equivalent to solve Equation (6) with $Q = 0$ and $P = (H^{(L-1)})^{(s)}W_L((H^{(L-1)})^{(t)}W_L)^\top$.*

The proof is in Appendix A. Proposition 1 shows that *BasicTFGM with GNN* is a special case of solving Equation (6): BasicTFGM sets node compatibility $Q = 0$ and uses a lower dimensional P . This shows training-free GNN's potential to approximate the structural term in graph matching.

Due to the BasicTFGM's limitation, we have proposed TFGM to preserve neighbor information of different orders and recover the node compatibility Q . For any matrix M , we define M_i to be the transpose of its i -th row vector. Let $\|\cdot\|_2$ represent the Euclidean norm and denote by the symbol " \odot " the element-wise multiplication. We show that *TFGM with GNN* is equivalent to solve Equation (6) with a specific choice of P and Q . Thus, we can summarize that TFGM is a linear relaxation of the QAP.

Proposition 2. *TFGM with $\text{GNN}_L(A, X)$ is equivalent to solve Equation (6) with $Q = Z^{(0)} \odot (X^{(s)}(X^{(t)})^\top)$ and $P^{(ij)} = \sum_{l=1}^L Z_{ij}^{(l)}(H^{(l-1)})^{(s)}W_l((H^{(l-1)})^{(t)}W_l)^\top$, where $Z^{(l)} \in \mathbb{R}^{|\mathcal{V}^{(s)}| \times |\mathcal{V}^{(t)}|}$ is the normalization matrix. $Z_{ij}^{(l)} = 1/(\|\text{GNN}_l(A^{(s)}, X^{(s)})_i\|_2\|\text{GNN}_l(A^{(t)}, X^{(t)})_j\|_2)$ for $l = 0, \dots, L$.*

4.3 Random-weight GNN v.s. Weight-free GNN (P3)

GA-MLPs (Chen et al., 2021) show that graph operators without nonlinear activation function can extract discriminative representations for node and graph classification. Based on their results, we conjecture that *it is inessential to use the nonlinear activation in training-free GNNs for graph matching*. Besides, one of the most important reasons for using activation function is to let neural networks learn complex nonlinear patterns. This reason does not hold when weights are not trained. Thus, we remove GNN's nonlinear activation function to investigate linear graph operators' effectiveness for graph matching. Specifically, we define the following random-weight GNN and weight-free GNN:

$$\begin{aligned} \text{Random-weight GNN}_L(A, X) &= A^L X W_1 \dots W_L; \\ \text{Weight-free GNN}_L(A, X) &= A^L X. \end{aligned}$$

Interestingly, we can prove that graph matching with the random-weight GNN approximates the weight-free GNN under the BasicTFGM framework (proof in Appendix A). The intuition is that the projection of a random matrix $W \sim \frac{1}{\sqrt{d}}\mathcal{N}(\mathbf{0}, \mathbf{I})$ can approximately preserve the distance between input vectors, which is well-known as the JL lemma (Johnson and Lindenstrauss, 1984; Shi et al., 2012).

The analysis above indicates that random-weight GNN should perform slightly worse than the weight-free GNN, which is demonstrated in experiments (Appendix C). Thus, we suggest the weight-free than the random-weight GNN.

4.4 Generalizing to Different Graph Operators (P4)

The adjacency matrix A in Equation (3) is a graph operator, which defines how GNN aggregate message from neighboring nodes. Let $\tilde{A} = A + I$ and $\tilde{D}_{ii} = \sum_j \tilde{A}_{ij}$. Proposition 1 and Proposition 2 can be generalized to other GCN-flavored GNNs like GCN (Kipf and Welling, 2017) and GraphSAGE (Hamilton et al., 2017) when using the

Table 2: Accuracy (%) of keypoint matching on PascalVOC. * denotes results from the original paper (Fey et al., 2020).

Methods	Aero	Bike	Bird	Boat	Bot.	Bus	Car	Cat	Cha.	Cow	Tab.	Dog	Hor.	MBike	Per.	Plant	Sheep	Sofa	Train	TV	Mean
NodeMatch	21.9	27.0	30.6	39.2	37.5	66.7	54.3	38.9	19.3	34.4	78.4	29.0	49.4	30.4	30.9	40.8	36.6	81.5	52.1	70.1	43.4
MLP*	34.3	45.9	37.3	47.7	53.3	75.2	64.5	61.7	27.7	40.5	85.9	46.6	50.2	39.0	37.3	58.0	49.2	82.9	65.0	74.2	53.8
GraphSAGE	33.8	39.8	36.6	53.1	54.9	79.7	64.2	49.6	28.6	49.1	83.4	41.9	56.3	34.5	37.6	62.0	46.7	81.4	65.4	77.5	53.8
SplineCNN*	42.1	57.5	49.6	59.4	83.8	84.0	78.4	67.5	37.3	60.4	85.0	58.0	66.0	54.1	52.6	93.9	60.2	85.6	87.8	82.5	67.3
DGMC*	47.0	65.7	56.8	67.6	86.9	87.7	85.3	72.6	42.9	69.1	84.5	63.8	78.1	55.6	58.4	98.0	68.4	92.2	94.5	85.5	73.0
TFGM																					
GraphSAGE	25.6	30.0	31.3	44.0	38.7	70.9	54.7	41.2	21.9	33.0	80.7	29.8	47.3	28.5	30.7	48.2	39.4	83.1	60.0	74.0	45.7
SplineCNN	25.9	37.7	38.4	58.3	68.0	83.2	70.1	48.1	29.3	43.5	82.8	37.3	59.6	37.6	38.4	73.9	44.1	93.6	79.1	80.3	56.5
DGMC	27.9	39.6	43.4	63.3	78.3	85.3	76.6	55.1	31.4	47.2	85.8	41.2	62.9	36.4	53.1	86.0	46.0	96.0	88.0	83.3	61.3
TFGMws																					
GraphSAGE	39.4	43.6	42.2	48.4	57.4	74.9	59.9	53.5	26.7	39.6	78.9	39.2	56.6	42.9	34.3	65.9	42.4	87.8	65.0	76.6	53.8
SplineCNN	48.2	65.0	49.2	61.2	84.9	83.6	80.4	62.3	50.1	62.0	86.4	54.5	67.6	64.4	53.0	97.0	58.3	97.1	93.7	84.7	70.2
DGMC	53.9	72.1	56.6	67.6	87.7	86.5	84.9	68.3	56.1	72.1	90.1	58.5	74.2	70.5	58.2	97.4	62.2	97.5	95.2	85.2	74.7

corresponding graph operator in the graph matching objective:

$$S^* = \operatorname{argmax}_{S \in \mathcal{T}} \sum_{\substack{i \in \mathcal{V}^{(s)} \\ j \in \mathcal{V}^{(t)}}} Q_{ij} S_{ij} + \sum_{\substack{i, i' \in \mathcal{V}^{(s)} \\ j, j' \in \mathcal{V}^{(t)}}} \hat{A}_{i, i'}^{(s)} \hat{A}_{j, j'}^{(t)} P_{i' j'}^{(ij)} S_{ij},$$

where $\hat{A} = \tilde{D}^{-1/2} \tilde{A} \tilde{D}^{-1/2}$ for GCN; $\hat{A} = \tilde{D}^{-1} \tilde{A}$ for GraphSAGE. Compared to Equation (6), the only difference is that the previous binary indicator of edge existence is now scaled by node degrees. By this generalization, we can apply TFGM with the popular GCN and GraphSAGE.

Generalizing to More Powerful GNNs. This TFGM approach is not limited by the GCN-flavored architecture for its principles are universal priors of graph matching. We have experimentally verified that other GNNs, *e.g.*, SplineCNN (Fey et al., 2018), also perform promisingly under TFGM. For further exploration, we feel more powerful graph operators (Corso et al., 2020) and representing semantic edge features (Gilmer et al., 2017) are promising directions for training-free graph matching.

5 Experiments

We experiment on three benchmarks under supervised, semi-supervised, and unsupervised settings. The experimental purpose is not to surpass the fully trained state-of-the-art, but to verify TFGM’s superiority for boosting GNNs’ performances under the training-free setting and provide empirical evidence of our analysis. We also conduct ablation studies to test TFGM’s key components and efficiency.

Experimental Setup. We use GraphSAGE (Hamilton et al., 2017), SplineCNN (Fey et al., 2018), and DGMC (Fey et al., 2020) as the baseline GNNs for TFGM due to their popularity in graph matching. To investigate the effectiveness of training and utilizing annotation (**P2**), we present GNNs’ performances of three versions: the original **fully trained version**, **TFGM**, and **TFGMws**. Note that the models in the following tables without TFGM or TFGMws are fully trained. We use the same LAP solver as the baselines in experiments for fair comparison. The detailed experimental setup is in Appendix C.2.

5.1 Supervised Keypoint Matching on Images

Keypoint matching is supervised graph matching to find the semantic equivalent keypoints between images of the same objects. We experiment on PascalVOC (Everingham et al., 2010) with Berkeley annotation (Bourdev and Malik, 2009), a benchmark with 20 categories of objects (Table 2).

First, TFGMws performs better than fully trained GNNs on mean accuracy. This demonstrates training-free methods’ ability to integrate node features and structure features. We attribute TFGMws’ better performance to the preserved neighborhood at different localities. TFGMws strictly compares nodes’ neighbors within the same order, while trained GNNs fail to guarantee such similarity measurement. Second, TFGMws shows significant improvement (11.7% on average) over TFGM. This implies the importance of annotation, and our proposed method can effectively utilize annotation without training. Third, TFGM benefits from advanced architectures: DGMC and SplineCNN significantly outperform GraphSAGE. This coincidences with **P4** that TFGM can capture the inductive bias in GNNs.

Table 3: Entity alignment performance on DBP15k. * indicates performance from original papers.

Methods	ZH-EN			JA-EN			FR-EN		
	H@1	H@10	MRR	H@1	H@10	MRR	H@1	H@10	MRR
NodeMatch	60.3	71.1	0.641	66.6	77.1	0.704	84.6	91.2	0.871
MLP	61.1	69.8	0.643	68.7	77.9	0.721	89.0	93.9	0.909
EVA*	76.1	90.7	0.814	76.2	91.3	0.817	79.3	94.2	0.847
NMN*	73.3	86.9	-	78.5	91.2	-	90.2	96.7	-
GraphSAGE	69.4	85.1	0.752	73.8	88.3	0.790	87.9	95.8	0.909
DGMC*	80.1	87.5	-	84.8	89.7	-	93.3	96.0	-
TFGM									
GraphSAGE	66.9	79.1	0.712	74.2	85.1	0.781	88.6	94.6	0.908
DGMC	79.1	84.5	0.811	84.6	90.5	0.869	94.4	97.0	0.954
TFGMws									
GraphSAGE	69.0	81.1	0.733	75.7	86.5	0.795	89.2	95.2	0.914
DGMC	81.4	86.3	0.833	86.2	91.5	0.883	94.9	97.3	0.959

Table 4: Accuracy (%) of Network Alignment on the PPI dataset. We report the baseline performances from our re-implementation with their released source code.

Noise Ratio	Low-conf. Edges					Random Rewirement				
	5%	10%	15%	20%	25%	5%	10%	15%	20%	25%
GHOST	73.6	48.9	36.7	25.5	20.4	41.7	14.9	11.6	9.2	7.5
KerGM	64.2	48.6	39.7	30.7	29.9	38.6	14.6	5.8	1.7	1.0
MAGNA++	74.0	66.3	58.4	49.8	43.3	67.2	44.6	36.9	34.1	30.6
TFGM one-hot										
GraphSAGE	65.1	46.2	32.1	29.1	23.5	83.3	81.1	78.1	75.0	71.7
DGMC	79.0	74.2	40.5	48.3	34.0	83.6	81.3	77.9	74.0	67.8
TFGM pos-enc										
GraphSAGE	79.9	62.6	52.7	41.1	33.2	75.5	67.1	59.5	53.2	45.3
DGMC	83.6	78.6	72.4	62.4	50.1	81.9	76.8	68.4	58.1	50.2

5.2 Semi-supervised Entity Alignment on KGs

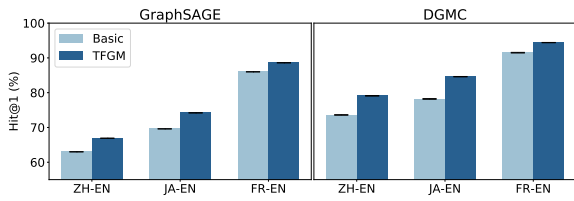
Entity alignment is semi-supervised graph matching aiming to find equivalent entities between two KGs. We use a benchmark DBP15k (Sun et al., 2017) with KGs between language pairs: Chinese to English (ZH-EN), Japanese to English (JA-EN), and French to English (FR-EN). We compare with unsupervised method EVA (Liu et al., 2021) and GNN model NMN (Wu et al., 2020). Table 3 presents performances of Hit@1 (H@1), Hit@10 (H@10) and Mean Reciprocal Rank (MRR).

First, *DGMC with TFGMws* outperforms its fully trained counterpart on 5 out of 6 metrics, demonstrating training-free methods’ ability to integrate node and structure features. Second, TFGM significantly outperforms the unsupervised baseline EVA and fully trained baseline NMN while enjoying an efficient training-free property. This performance demonstrates TFGM’s superiority in the unsupervised setting. Note that EVA uses extra visual features, which significantly boost the Hit@10 scores. Third, TFGMws outperforms TFGM by only 1.4% Hit@1 on average. Compared with supervised graph matching (Table 2), the improvement is limited. We attribute this to the weak supervision in DBP15k: the unsupervised baseline EVA’s performance is very competitive to supervised baselines. In addition, shown by the decent performance of NodeMatch, the initial node features are strong for measuring semantic equivalence.

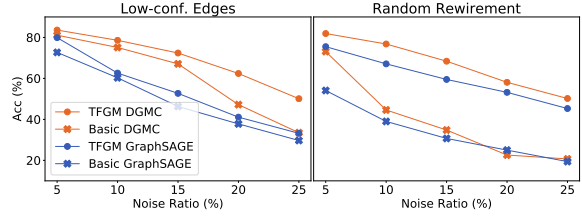
5.3 Unsupervised Network Alignment of Protein-Protein Interaction Networks

Protein-Protein Interaction (PPI) Network Alignment is unsupervised and aims to find corresponding proteins in networks of different species. We use the Low-conf. Edges dataset (Collins et al., 2007) and Random Rewirement dataset (Saraph and Milenković, 2014) for evaluation. Each dataset has 5 versions of different noise ratios. We compare with unsupervised baselines GHOST (Patro and Kingsford, 2012), KerGM (Zhang et al., 2019b), and MAGNA++ (Vijayan et al., 2015). This dataset has no node features. We thus initialize the nodes with the one-hot encoding or positional-encoding (Vaswani et al., 2017) of node degrees. Table 4 reports the matching accuracy.

First, we can see that TFGM outperforms baselines by a large margin (17.7% on average), demonstrating the superiority of TFGM in the unsupervised setting. We attribute the good performance to TFGM’s effectiveness in capturing high-



(a) Training-free GNNs' performance on DBP15k.



(b) Training-free GNNs with positional encoding on PPI.

Figure 2: Comparison of the TFGM and the BasicTFGM.

order neighborhoods with deep GNNs (*i.e.*, 10 layers). Baselines use only one-hop neighbors of nodes. Second, TFGM one-hot performs best among models on the Random Rewirement dataset. This is because this dataset is generated while ensuring equivalent nodes to have the same degree, which provides a strong bias for one-hot matching. As a note, NodeMatch that compares only degree features has accuracy $< 10\%$ due to duplicate degrees. Third, GraphSAGE outperforms DGMC on the Random Rewirement dataset if using one-hot encoding. This is expected because the “rewirement” noise violates the structural consistency, thus confuses DGMC’s refinement towards the consistency.

Discussion. PPI dataset has no node features, thus matching relies on the assumption of structural consistency (Wang et al., 2018). On the Low-conf. Edges dataset, this assumption holds exactly because the source graph is a subgraph of the target graph. Therefore, optimizing QAP (Equation (1)) guarantees the optimal performance on the Low-conf. Edges dataset. Our experiments on it give empirical evaluation for TFGM’s approximation of the QAP objective.

5.4 Ablation Studies

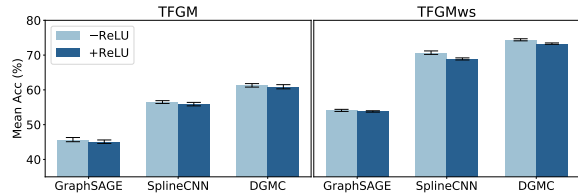
Preserving Neighbors of Different Localities. To further demonstrate the importance of preserving neighbors of different orders, we compare training-free GNNs under different frameworks: BasicTFGM based on the L -th order neighborhoods and TFGM based on all of $(0, 1, \dots, L)$ -th orders’ neighborhoods. For BasicTFGM, we use residual connection (He et al., 2016) to preserve the node compatibility. Figure 2 shows that GNNs under the TFGM framework consistently outperform their BasicTFGM counterparts (4.3% on average on DBP15k, 16.7% on average on PPI). We observe similar results on PascalVOC (Appendix C.1).

Efficiency. We present the average running time in Table 5 to evaluate TFGM’s efficiency. We compare models with the best performance to obtain the most representative results. For baselines, we use DGMC on PascalVOC and DBP15k and use MAGNA++ on PPI. For our framework, we stick with DGMC as the backbone GNN.

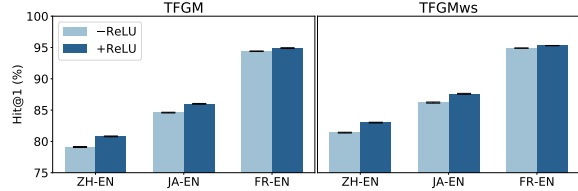
First, we highlight that our framework performs empirically faster than all baselines by a large margin. On PascalVOC and DBP15k, TFGMws is $7 \sim 8$ times faster than the fully trained models due to the cut-down of the training phase. On PPI, TFGM is nearly 5000 times faster than MAGNA++ due to TFGM’s efficiency and GPU acceleration. Second, TFGM further improves over TFGMws on speed for not relying on training data. Considering TFGM’s better performance than some supervised models in experiments (Table 2, 3), it makes a fast promising solution for graph

Table 5: Average running time (seconds) of 5 independent runs for the best performing baselines, TFGM, and TFGMws. We do not count the time for loading datasets.

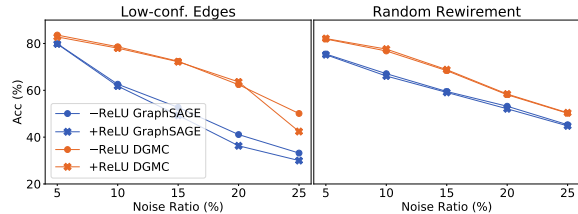
Dataset	BestBaseline	TFGM	TFGMws
PascalVOC	504.3	18.1	67.2
DBP15k	44.1	5.5	5.7
PPI	983.0	0.2	-



(a) TFGM with GNNs on PascalVOC.



(b) TFGM with DGMC on DBP15k.



(c) TFGM pos-enc with GNNs on PPI.

Figure 3: TFGM’s performance with and without ReLU.

matching. Third, the gap between TFGM and TFGMws is small on DBP15k, showing that our strategy for utilizing annotation introduces little computation overhead in the semi-supervised setting. Complexity analysis is in Appendix B.

Removing Nonlinear Activation. We now support our conjecture that *it is inessential to use the nonlinear activation in training-free GNNs for graph matching* (Section 4.3) with empirical evidence. In Figure 3, we compare TFGM’s performance with and without the ReLU nonlinearity, the most common activation function. ReLU’s contribution to performance is unstable across datasets: on PascalVOC, without ReLU is better; on DBP15k, with ReLU is better; on PPI, ReLU makes no significant difference. We conclude that ReLU is inessential in the training-free setting.

6 Conclusion and Future Work

We present the first framework TFGM for graph matching with training-free GNNs. TFGM provides a fast approximate solution to graph matching without training. We handcraft matching priors, which used be learned by training, into GNN’s architecture and show that TFGM is a linear relaxation to graph matching’s QAP formulation. Extensive experiments demonstrate TFGM’s generalizability to supervised, semi-supervised, and unsupervised graph matching. Further ablation studies validate TFGM’s key components. In the future, we are interested in exploring training-free GNNs for zero-shot learning.

References

- Max Berrendorf, Evgeniy Faerman, and Volker Tresp. Active learning for entity alignment. In *European Conference on Information Retrieval*, pages 48–62. Springer, 2021.
- Vincent D Blondel, Jean-Loup Guillaume, Renaud Lambiotte, and Etienne Lefebvre. Fast unfolding of communities in large networks. *Journal of Statistical Mechanics: Theory and Experiment*, 2008(10), 2008.
- Lubomir Bourdev and Jitendra Malik. Poselets: Body part detectors trained using 3d human pose annotations. In *ICCV*, 2009.
- Tib rio S Caetano, Julian J McAuley, Li Cheng, Quoc V Le, and Alex J Smola. Learning graph matching. *IEEE Transactions on Pattern Analysis and Machine Intelligence*, 31(6), 2009.
- Hwann-Tzong Chen, Horng-Horng Lin, and Tyng-Luh Liu. Multi-object tracking using dynamical graph matching. In *CVPR*. IEEE, 2001.
- Lei Chen, Zhengdao Chen, and Joan Bruna. On graph neural networks versus graph-augmented mlps. In *ICLR*, 2021.
- Muhao Chen, Yingtao Tian, Mohan Yang, and Carlo Zaniolo. Multilingual knowledge graph embeddings for cross-lingual knowledge alignment. In *IJCAI*, 2016.
- Ting Chen, Song Bian, and Yizhou Sun. Are powerful graph neural nets necessary? a dissection on graph classification. *arXiv preprint arXiv:1905.04579*, 2019.
- Wei-Lin Chiang, Xuanqing Liu, Si Si, Yang Li, Samy Bengio, and Cho-Jui Hsieh. Cluster-gcn: An efficient algorithm for training deep and large graph convolutional networks. In *SIGKDD*, 2019.
- Minsu Cho, Karteek Alahari, and Jean Ponce. Learning graphs to match. In *ICCV*, 2013.
- Christopher B Choy, JunYoung Gwak, Silvio Savarese, and Manmohan Chandraker. Universal correspondence network. In *NeurIPS*, 2016.
- Xiaokai Chu, Xinxin Fan, Di Yao, Zhihua Zhu, Jianhui Huang, and Jingping Bi. Cross-network embedding for multi-network alignment. In *World Wide Web Conference*, pages 273–284, 2019.
- Sean R Collins, Patrick Kemmeren, Xue-Chu Zhao, Jack F Greenblatt, Forrest Spencer, Frank CP Holstege, Jonathan S Weissman, and Nevan J Krogan. Toward a comprehensive atlas of the physical interactome of *saccharomyces cerevisiae*. *Molecular & Cellular Proteomics*, 6(3), 2007.
- Donatello Conte, Pasquale Foggia, Carlo Sansone, and Mario Vento. Thirty years of graph matching in pattern recognition. *International Journal of Pattern Recognition and Artificial Intelligence*, 2004.
- Gabriele Corso, Luca Cavalleri, Dominique Beaini, Pietro Li , and Petar Veli kovi . Principal neighbourhood aggregation for graph nets. In *NeurIPS*, 2020.

- Marco Cuturi. Sinkhorn distances: Lightspeed computation of optimal transport. *NIPS*, 2013.
- Ahed Elmsallati, Connor Clark, and Jugal Kalita. Global alignment of protein-protein interaction networks: A survey. *IEEE/ACM Transactions on Computational Biology and Bioinformatics*, 13(4), 2015.
- Mark Everingham, Luc Van Gool, Christopher KI Williams, John Winn, and Andrew Zisserman. The pascal visual object classes (voc) challenge. *IJCV*, 2010.
- Fazle E Faisal, Lei Meng, Joseph Crawford, and Tijana Milenković. The post-genomic era of biological network alignment. *EURASIP Journal on Bioinformatics and Systems Biology*, 2015(1), 2015.
- Matthias Fey, Jan Eric Lenssen, Frank Weichert, and Heinrich Müller. Splinecnn: Fast geometric deep learning with continuous b-spline kernels. In *CVPR*, 2018.
- Matthias Fey, Jan E Lenssen, Christopher Morris, Jonathan Masci, and Nils M Kriege. Deep graph matching consensus. In *ICLR*, 2020.
- Stephen P Ficklin and F Alex Feltus. Gene coexpression network alignment and conservation of gene modules between two grass species: maize and rice. *Plant Physiology*, 156, 2011.
- Fabrizio Frasca, Emanuele Rossi, Davide Eynard, Ben Chamberlain, Michael Bronstein, and Federico Monti. Sign: Scalable inception graph neural networks. *arXiv preprint arXiv:2004.11198*, 2020.
- Justin Gilmer, Samuel S Schoenholz, Patrick F Riley, Oriol Vinyals, and George E Dahl. Neural message passing for quantum chemistry. In *ICML*, pages 1263–1272, 2017.
- Rohit Girdhar, Georgia Gkioxari, Lorenzo Torresani, Manohar Paluri, and Du Tran. Detect-and-track: Efficient pose estimation in videos. In *CVPR*, pages 350–359, 2018.
- Will Hamilton, Zhitao Ying, and Jure Leskovec. Inductive representation learning on large graphs. In *NeurIPS*, 2017.
- Kaiming He, Xiangyu Zhang, Shaoqing Ren, and Jian Sun. Deep residual learning for image recognition. In *CVPR*, 2016.
- Guang-Bin Huang, Lei Chen, Chee Kheong Siew, et al. Universal approximation using incremental constructive feedforward networks with random hidden nodes. *IEEE Transactions on Neural Networks*, 17(4), 2006.
- Boris Igel'nik and Yoh-Han Pao. Stochastic choice of basis functions in adaptive function approximation and the functional-link net. *IEEE Transactions on Neural Networks*, 6(6), 1995.
- Kevin Jarrett, Koray Kavukcuoglu, Marc' Aurelio Ranzato, and Yann LeCun. What is the best multi-stage architecture for object recognition? In *ICCV*, 2009.
- William B Johnson and Joram Lindenstrauss. Extensions of lipschitz mappings into a hilbert space. *Contemporary Mathematics*, 26(189-206), 1984.
- Thomas N Kipf and Max Welling. Semi-supervised classification with graph convolutional networks. In *ICLR*, 2017.
- Jin-Yan Li, Wing Sun Chow, Boris Igel'nik, and Yoh-Han Pao. Comments on " stochastic choice of basis functions in adaptive function approximation and the functional-link net"[with reply]. *IEEE Transactions on Neural Networks*, 8 (2), 1997.
- Fangyu Liu, Muhao Chen, Dan Roth, and Nigel Collier. Visual pivoting for (unsupervised) entity alignment. In *AAAI*, 2021.
- Xin Mao, Wenting Wang, Yuanbin Wu, and Man Lan. Boosting the speed of entity alignment 10×: Dual attention matching network with normalized hard sample mining. In *The Web Conference*, pages 821–832, 2021.
- Gonzalo Mena, David Belanger, Gonzalo Munoz, and Jasper Snoek. Sinkhorn networks: Using optimal transport techniques to learn permutations. In *NIPS Workshop in Optimal Transport and Machine Learning*, volume 3, 2017.
- Hoang Nt and Takanori Maehara. Revisiting graph neural networks: All we have is low-pass filters. *arXiv preprint arXiv:1905.09550*, 2019.
- Rob Patro and Carl Kingsford. Global network alignment using multiscale spectral signatures. *Bioinformatics*, 28, 2012.

- Nils Reimers and Iryna Gurevych. Sentence-bert: Sentence embeddings using siamese bert-networks. In *EMNLP*, 2019.
- Ignacio Rocco, Mircea Cimpoi, Relja Arandjelović, Akihiko Torii, Tomas Pajdla, and Josef Sivic. Neighbourhood consensus networks. In *NeurIPS*, 2018.
- Michal Rolínek, Paul Swoboda, Dominik Zietlow, Anselm Paulus, Vít Musil, and Georg Martius. Deep graph matching via blackbox differentiation of combinatorial solvers. In *ECCV*, 2020.
- Vikram Saraph and Tijana Milenković. Magna: maximizing accuracy in global network alignment. *Bioinformatics*, 30, 2014.
- Paul-Edouard Sarlin, Daniel DeTone, Tomasz Malisiewicz, and Andrew Rabinovich. Superglue: Learning feature matching with graph neural networks. In *CVPR*, 2020.
- Andrew M Saxe, Pang Wei Koh, Zhenghao Chen, Maneesh Bhand, Bipin Suresh, and Andrew Y Ng. On random weights and unsupervised feature learning. In *ICML*, 2011.
- Qinfeng Shi, Chunhua Shen, Rhys Hill, and Anton van den Hengel. Is margin preserved after random projection? In *ICML*, 2012.
- Karen Simonyan and Andrew Zisserman. Very deep convolutional networks for large-scale image recognition. *arXiv preprint arXiv:1409.1556*, 2014.
- Zequn Sun, Wei Hu, and Chengkai Li. Cross-lingual entity alignment via joint attribute-preserving embedding. In *ISWC*, 2017.
- Zequn Sun, Qingheng Zhang, Wei Hu, Chengming Wang, Muhao Chen, Farahnaz Akrami, and Chengkai Li. A benchmarking study of embedding-based entity alignment for knowledge graphs. *arXiv preprint arXiv:2003.07743*, 2020.
- Paul Swoboda, Carsten Rother, Hassan Abu Alhaija, Dagmar Kainmuller, and Bogdan Savchynskyy. A study of lagrangean decompositions and dual ascent solvers for graph matching. In *CVPR*, 2017.
- Paul Swoboda, Ashkan Mokarian, Christian Theobalt, Florian Bernard, et al. A convex relaxation for multi-graph matching. In *CVPR*, 2019.
- Dmitry Ulyanov, Andrea Vedaldi, and Victor Lempitsky. Deep image prior. In *CVPR*, 2018.
- Ashish Vaswani, Noam Shazeer, Niki Parmar, Jakob Uszkoreit, Llion Jones, Aidan N Gomez, Lukasz Kaiser, and Illia Polosukhin. Attention is all you need. In *NIPS*, 2017.
- Vipin Vijayan, Vikram Saraph, and Tijana Milenković. Magna++: Maximizing accuracy in global network alignment via both node and edge conservation. *Bioinformatics*, 31, 2015.
- Oriol Vinyals, Charles Blundell, Timothy Lillicrap, Koray Kavukcuoglu, and Daan Wierstra. Matching networks for one shot learning. In *NIPS*, 2016.
- Runzhong Wang, Junchi Yan, and Xiaokang Yang. Learning combinatorial embedding networks for deep graph matching. In *ICCV*, 2019a.
- Runzhong Wang, Junchi Yan, and Xiaokang Yang. Neural graph matching network: Learning lawler’s quadratic assignment problem with extension to hypergraph and multiple-graph matching. *IEEE Transactions on Pattern Analysis and Machine Intelligence*, 2019b.
- Yue Wang and Justin M Solomon. Deep closest point: Learning representations for point cloud registration. In *ICCV*, pages 3523–3532, 2019.
- Zhichun Wang, Qingsong Lv, Xiaohan Lan, and Yu Zhang. Cross-lingual knowledge graph alignment via graph convolutional networks. In *EMNLP*, 2018.
- Felix Wu, Amauri Souza, Tianyi Zhang, Christopher Fifty, Tao Yu, and Kilian Weinberger. Simplifying graph convolutional networks. In *ICML*, 2019.
- Yuting Wu, Xiao Liu, Yansong Feng, Zheng Wang, and Dongyan Zhao. Neighborhood matching network for entity alignment. In *ACL*, 2020.

- Kun Xu, Liwei Wang, Mo Yu, Yansong Feng, Yan Song, Zhiguo Wang, and Dong Yu. Cross-lingual knowledge graph alignment via graph matching neural network. In *ACL*, 2019.
- Yuchen Yan, Si Zhang, and Hanghang Tong. Bright: A bridging algorithm for network alignment. In *The Web Conference*, pages 3907–3917, 2021.
- Daniele Zambon, Cesare Alippi, and Lorenzo Livi. Graph random neural features for distance-preserving graph representations. In *ICML*. PMLR, 2020.
- Andrei Zanfir and Cristian Sminchisescu. Deep learning of graph matching. In *CVPR*, 2018.
- Jiawei Zhang and S Yu Philip. Multiple anonymized social networks alignment. In *ICDM*, pages 599–608. IEEE, 2015.
- Si Zhang, Hanghang Tong, Ross Maciejewski, and Tina Eliassi-Rad. Multilevel network alignment. In *The World Wide Web Conference*, pages 2344–2354, 2019a.
- Zhen Zhang, Yijian Xiang, Lingfei Wu, Bing Xue, and Arye Nehorai. Kergm: Kernelized graph matching. In *NeurIPS*, 2019b.
- Xiang Zhao, Weixin Zeng, Jiuyang Tang, Wei Wang, and Fabian Suchanek. An experimental study of state-of-the-art entity alignment approaches. *TKDE*, 2020.
- Zexuan Zhong, Yong Cao, Mu Guo, and Zaiqing Nie. Colink: An unsupervised framework for user identity linkage. In *AAAI*, 2018.
- Qinghai Zhou, Liangyue Li, Xintao Wu, Nan Cao, Lei Ying, and Hanghang Tong. Attent: Active attributed network alignment. In *The Web Conference*, pages 3896–3906, 2021.
- Qi Zhu, Hao Wei, Bunyamin Sisman, Da Zheng, Christos Faloutsos, Xin Luna Dong, and Jiawei Han. Collective multi-type entity alignment between knowledge graphs. In *The Web Conference*, pages 2241–2252, 2020.
- Difan Zou, Ziniu Hu, Yewen Wang, Song Jiang, Yizhou Sun, and Quanquan Gu. Layer-dependent importance sampling for training deep and large graph convolutional networks. In *NeurIPS*, 2019.

Supplementary Material for Training-Free Graph Neural Networks for Graph Matching

A Proofs

Proof of Proposition 1:

Proof. Let $\phi(\mathcal{G}) = \text{GNN}_L(A, X)$, we need to show that Eq. 4 can be rewritten as Eq. 6:

$$\begin{aligned} S^* &= \operatorname{argmax}_{S \in \mathcal{T}} \sum_{\substack{i \in \mathcal{V}^{(s)} \\ j \in \mathcal{V}^{(t)}}} S_{ij} \left(\text{GNN}_L(A^{(s)}, X^{(s)}) \text{GNN}_L(A^{(t)}, X^{(t)})^\top \right)_{ij} \\ &= \operatorname{argmax}_{S \in \mathcal{T}} \sum_{\substack{i \in \mathcal{V}^{(s)} \\ j \in \mathcal{V}^{(t)}}} S_{ij} \left((A^{(s)}(H^{(L-1)})^{(s)}W_L)(A^{(t)}(H^{(L-1)})^{(t)}W_L)^\top \right)_{ij} \end{aligned}$$

Substitute $P = (H^{(L-1)})^{(s)}W_L((H^{(L-1)})^{(t)}W_L)^\top$:

$$\begin{aligned} S^* &= \operatorname{argmax}_{S \in \mathcal{T}} \sum_{i \in \mathcal{V}^{(s)}, j \in \mathcal{V}^{(t)}} S_{ij} (A^{(s)}P(A^{(t)})^\top)_{ij} \\ &= \operatorname{argmax}_{S \in \mathcal{T}} \sum_{i, i' \in \mathcal{V}^{(s)}, j, j' \in \mathcal{V}^{(t)}} A_{ii'}^{(s)} A_{jj'}^{(t)} S_{ij} P_{i'j'} \end{aligned}$$

□

Proof of Proposition 2:

Proof. Let $g_l(\mathcal{G}) = \text{GNN}_L(A, X)$, we need to rewrite Equation (5) as Equation (6).

For any matrix $B \in \mathbb{R}^{n \times m}$, we define $B_{i:} \in \mathbb{R}^{1 \times m}$ to be its i -th row vector for $i = 1, \dots, n$. Let $M_{ij}^{(l)} = 1/Z_{ij}^{(l)}$. Let S^* be the solution of *TFGM* with $\text{GNN}_L(A, X)$. Then, by the definition of the cosine similarity and the linearity of matrix indexing,

$$\begin{aligned} S^* &= \operatorname{argmax}_{S \in \mathcal{T}} \sum_{\substack{i \in \mathcal{V}^{(s)} \\ j \in \mathcal{V}^{(t)}}} S_{ij} \left(\sum_{l=0}^L \text{Cos} \left(\text{GNN}_l(A^{(s)}, X^{(s)}), \text{GNN}_l(A^{(t)}, X^{(t)}) \right) \right)_{ij} \\ &= \operatorname{argmax}_{S \in \mathcal{T}} \sum_{\substack{i \in \mathcal{V}^{(s)} \\ j \in \mathcal{V}^{(t)}}} S_{ij} \sum_{l=0}^L \frac{\langle \text{GNN}_l(A^{(s)}, X^{(s)})_{i:}, \text{GNN}_l(A^{(t)}, X^{(t)})_{j:} \rangle}{M_{ij}^{(l)}} \end{aligned}$$

For the $l = 0$ term,

$$\frac{\langle \text{GNN}_0(A^{(s)}, X^{(s)})_{i:}, \text{GNN}_0(A^{(t)}, X^{(t)})_{j:} \rangle}{M_{ij}^{(0)}} = \frac{\langle X_{i:}^{(s)}, X_{j:}^{(t)} \rangle}{M_{ij}^{(0)}} = Q_{ij}.$$

For the $l \geq 1$ term,

$$\begin{aligned}
& \sum_{l=1}^L \frac{\langle A_{i:}^{(s)} (H^{(l-1)})^{(s)} W_L, A_{j:}^{(t)} (H^{(l-1)})^{(t)} W_L \rangle}{M_{ij}^{(l)}} \\
&= \sum_{l=1}^L \frac{\sum_{i' \in \mathcal{V}^{(s)}, j' \in \mathcal{V}^{(t)}} A_{ii'}^{(s)} A_{jj'}^{(t)} \left((H^{(l-1)})^{(s)} W_L ((H^{(l-1)})^{(t)} W_L)^\top \right)_{i'j'}}{M_{ij}^{(l)}} \\
&= \sum_{\substack{i' \in \mathcal{V}^{(s)} \\ j' \in \mathcal{V}^{(t)}}} A_{ii'}^{(s)} A_{jj'}^{(t)} \left(\sum_{l=1}^L \frac{1}{M_{ij}^{(l)}} (H^{(l-1)})^{(s)} W_L ((H^{(l-1)})^{(t)} W_L)^\top \right)_{i'j'} \\
&= \sum_{\substack{i' \in \mathcal{V}^{(s)} \\ j' \in \mathcal{V}^{(t)}}} A_{ii'}^{(s)} A_{jj'}^{(t)} P_{i'j'}^{(ij)}
\end{aligned}$$

By combining those, we have that

$$S^* = \operatorname{argmax}_{S \in \mathcal{T}} \sum_{i \in \mathcal{V}^{(s)}, j \in \mathcal{V}^{(t)}} S_{ij} Q_{ij} + \sum_{\substack{i, i' \in \mathcal{V}^{(s)} \\ j, j' \in \mathcal{V}^{(t)}}} A_{ii'}^{(s)} A_{jj'}^{(t)} P_{i'j'}^{(i,j)} S_{ij},$$

which proves the desired statement. \square

Proof of that graph matching with the random-weight GNN approximates the weight-free GNN under the BasicTFGM framework.

Proof. Based on Proposition 1, it is easy to show that the objective of *BasicTFGM with random-weight GNN and weight-free GNN* can also be aligned with Equation (6). In specific, we have $Q_0 = 0$ and $P_0 = (A^{(s)})^{L-1} X^{(s)} W_1 \dots W_L ((A^{(t)})^{L-1} X^{(t)} W_1 \dots W_L)^\top$ for random-weight GNN; and $Q_1 = 0$ and $P_1 = (A^{(s)})^{L-1} X^{(s)} ((A^{(t)})^{L-1} X^{(t)})^\top$ for weight-free GNN.

To show that random-weight GNN approximates the weight-free GNN under the BasicTFGM framework, we need to show that P_0 is an unbiased estimator of P_1 :

$$P_1 = \mathbb{E}_{\{W_l\}_1^L \sim \frac{1}{\sqrt{d}} \mathcal{N}(\mathbf{0}, \mathbf{I})} [P_0],$$

In Section 3.1, we define weights $\{W_l\}_1^L$ to be sampled from $\frac{1}{\sqrt{d}} \mathcal{N}(\mathbf{0}, \mathbf{I})$. Thus, we have:

$$\mathbb{E}_{\{W_l\}_1^L} [P_0] = \mathbb{E}[\left((A^{(s)})^{L-1} X^{(s)} W_1 \dots W_L \right) \left((A^{(t)})^{L-1} X^{(t)} W_1 \dots W_L \right)^\top] \quad (7)$$

$$= (A^{(s)})^{L-1} X^{(s)} \mathbb{E}[W_1 \dots W_L W_L^\top \dots W_1^\top] \left((A^{(t)})^{L-1} X^{(t)} \right)^\top \quad (8)$$

Let $K_L = W_1 \dots W_L W_L^\top \dots W_1^\top$, we prove by induction that

$$\mathbb{E}[K_L] = I, \text{ for any integer } L > 0. \quad (9)$$

Base case: $L = 1$, it is easy to show that $\mathbb{E}[K_1] = \mathbb{E}[W_1 W_1^\top] = I$ (using the independence of random variables).

Inductive step: suppose Eq. 9 holds for $L - 1$, i.e., $\mathbb{E}[K_{L-1}] = I$.

Let $B_{L-1} = W_1 \dots W_{L-1}$, then we have $K_L = B_{L-1} W_L W_L^\top B_{L-1}^\top$ and

$$\begin{aligned}
\mathbb{E}[(K_L)_{ij}] &= \mathbb{E}\left[\sum_k (B_{L-1} W_L)_{ik} (B_{L-1} W_L)_{jk} \right] \\
&= \mathbb{E}\left[\sum_{k,a,b} (B_{L-1})_{ia} (W_L)_{ak} (B_{L-1})_{jb} (W_L)_{bk} \right] \\
&= \sum_{k,a,b} \mathbb{E}[(B_{L-1})_{ia} (W_L)_{ak} (B_{L-1})_{jb} (W_L)_{bk}] \\
&= \sum_{k,a,b} \mathbb{E}[(B_{L-1})_{ia} (B_{L-1})_{jb}] \mathbb{E}[(W_L)_{ak} (W_L)_{bk}]
\end{aligned}$$

If $i \neq j, a \neq b$,

$$\begin{aligned} & \mathbb{E}[(B_{L-1})_{ia}(B_{L-1})_{jb}]\mathbb{E}[(W_L)_{ak}(W_L)_{bk}] \\ & = \mathbb{E}[(B_{L-1})_{ia}(B_{L-1})_{jb}]\mathbb{E}[(W_L)_{ak}]\mathbb{E}[(W_L)_{bk}] = 0 \end{aligned}$$

If $i \neq j, a = b$,

$$\begin{aligned} & \mathbb{E}[(B_{L-1})_{ia}(B_{L-1})_{jb}]\mathbb{E}[(W_L)_{ak}(W_L)_{bk}] \\ & = \mathbb{E}[(B_{L-1})_{ia}(B_{L-1})_{jb}]\mathbb{E}[(W_L)_{ak}^2] = \frac{1}{d}\mathbb{E}[(B_{L-1})_{ia}(B_{L-1})_{jb}] \end{aligned}$$

If $i = j, a \neq b$,

$$\mathbb{E}[(B_{L-1})_{ia}(B_{L-1})_{jb}]\mathbb{E}[(W_L)_{ak}(W_L)_{bk}] = 0$$

If $i = j, a = b$,

$$\begin{aligned} & \mathbb{E}[(B_{L-1})_{ia}(B_{L-1})_{jb}]\mathbb{E}[(W_L)_{ak}(W_L)_{bk}] \\ & = \mathbb{E}[(B_{L-1})_{ia}^2]\mathbb{E}[(W_L)_{ak}^2] = \frac{1}{d}\mathbb{E}[(B_{L-1})_{ia}^2] \end{aligned}$$

Thus, for K_L , if $i \neq j$,

$$\begin{aligned} \mathbb{E}[(K_L)_{ij}] & = \sum_{k,a} \frac{1}{d}\mathbb{E}[(B_{L-1})_{ia}(B_{L-1})_{ja}] \\ & = \sum_a \mathbb{E}[(B_{L-1})_{ia}(B_{L-1})_{ja}] = \mathbb{E}[(K_{L-1})_{ij}] = 0 \end{aligned}$$

If $i = j$,

$$\mathbb{E}[(K_L)_{ii}] = \sum_{k,a} \frac{1}{d}\mathbb{E}[(B_{L-1})_{ia}^2] = \sum_a \mathbb{E}[(B_{L-1})_{ia}^2] = \mathbb{E}[(K_{L-1})_{ii}] = 1$$

We conclude that $\mathbb{E}[K_L] = I$ for all integer $L > 0$. Substitute this into Eq. 8, we have $P_1 = \mathbb{E}_{\{W_i\}_{i=1}^L \sim \frac{1}{\sqrt{d}}\mathcal{N}(\mathbf{0}, \mathbf{I})} [P_0]$. \square

B Complexity Analysis

We now analyze the complexity of graph matching using a GCN-flavored weight-free GNN under our framework. Let L be the number of GNN layers. d is the dimension of node feature. Given two graphs $\mathcal{G}^{(s)}$ and $\mathcal{G}^{(t)}$, let $\|A\|_0 = \max(\|A^{(s)}\|_0, \|A^{(t)}\|_0)$, $|\mathcal{V}| = \max(|\mathcal{V}^{(s)}|, |\mathcal{V}^{(t)}|)$. The complexity analysis is shown in Table 6.

Table 6: Complexity for graph matching with GCN-flavored weight-free GNN. The underlined part is the complexity for running a Hungarian solver of the LAP, which is optional.

	Unsupervised	Semi-supervised	Supervised
TFGM	$O(dL \mathcal{V} ^2) + \underline{O(\mathcal{V} ^3)}$	-	-
TFGM _{ws}	-	$O(dL \mathcal{V} ^2) + \underline{O(\mathcal{V} ^3)}$	$O(dL \mathcal{V} \sum_{i=1}^N \mathcal{V}^{(i)}) + O(N \log(N) \mathcal{V}) + \underline{O(\mathcal{V} ^3)}$

TFGM’s complexity is independent of training dataset size, making it a fast solution for graph matching.

The unsupervised and semi-supervised settings have the same complexity, because our strategy of using semi-supervised annotation is $O(d|\mathcal{I}|)$, where \mathcal{I} is the set of known equivalent node pairs. $O(d|\mathcal{I}|)$ is smaller than $O(d|\mathcal{V}|)$ and thus ignored.

We include the complexity of an optional Hungarian solver of LAP. If Hungarian is used, it dominates the complexity in the unsupervised and semi-supervised setting. However, running GNNs usually costs longer time than running the Hungarian in practice. We can use the less expensive argmax as LAP solver to achieve $O(dL|\mathcal{V}|^2)$ complexity.

In the supervised setting, we conduct kNN search in a training dataset $\mathcal{D} = \{\mathcal{G}^{(1)}, \dots, \mathcal{G}^{(N)}\}$. We assume that the graph matching with the training data uses the argmax LAP solver for efficiency. The complexity is dominated by two components: 1) graph matching between $\mathcal{G}^{(s)}$ and $\mathcal{G}^{(t)}$ and every graph in the training dataset; 2) sort the similarity scores to find the top k similar nodes. Empirically, the complexity is dominated by the first term $O(dL|\mathcal{V}|\sum_{i=1}^N |\mathcal{V}^{(i)}|)$, which is of the same magnitude or smaller than the fully trained models. However, once being trained, fully trained model performs much faster in the inference phase. We make it a future work to find a more efficient training-free method for the supervised setting.

C Experiments

C.1 Additional Results

BasicTFGM on PascalVOC. Table 7 compares the performance of BasicTFGM and TFGM on the supervised graph matching benchmark PascalVOC. TFGM with the three GNNs improves 6.4% on average compared to BasicTFGM. Compare to the BasicTFGM, the only difference is that TFGM concatenates the normalized output from all layers as node embedding. This result again demonstrates the importance of preserving neighbors of all orders for graph matching.

Table 7: Accuracy (%) of keypoint matching on PascalVOC.

Methods	Aero	Bike	Bird	Boat	Bot.	Bus	Car	Cat	Cha.	Cow	Tab.	Dog	Hor.	MBike	Per.	Plant	Sheep	Sofa	Train	TV	Mean
BasicTFGM																					
GraphSAGE	21.9	24.6	25.4	35.7	29.4	55.0	47.2	36.5	18.9	26.9	82.4	25.3	42.6	23.8	25.3	34.9	35.4	79.0	44.5	57.1	38.6
SplineCNN	27.2	31.8	34.3	46.2	45.5	71.4	57.4	43.9	25.6	34.1	79.7	30.4	52.2	28.9	36.0	49.4	40.3	86.7	58.5	73.5	47.7
DGMC	30.3	42.1	43.0	56.1	65.0	82.7	71.9	53.7	27.8	43.8	84.3	38.4	64.5	40.3	46.3	70.7	48.9	93.0	76.9	81.5	58.1
TFGM																					
GraphSAGE	25.6	30.0	31.3	44.0	38.7	70.9	54.7	41.2	21.9	33.0	80.7	29.8	47.3	28.5	30.7	48.2	39.4	83.1	60.0	74.0	45.7
SplineCNN	25.9	37.7	38.4	58.3	68.0	83.2	70.1	48.1	29.3	43.5	82.8	37.3	59.6	37.6	38.4	73.9	44.1	93.6	79.1	80.3	56.5
DGMC	27.9	39.6	43.4	63.3	78.3	85.3	76.6	55.1	31.4	47.2	85.8	41.2	62.9	36.4	53.1	86.0	46.0	96.0	88.0	83.3	61.3

Case Study. In Figure 2, TFGM has shown significant improvement over BasicTFGM. Thus, we conjecture that preserving information from different localities is crucial for obtaining structural representation in the training-free setting. We verify this conjecture in this case study. In Figure 4, we visualize the node embeddings obtained by training-free GCNs on the Karate club network, a similar case study as in (Kipf and Welling, 2017). Specifically, we present a TFGM-flavored weight-free GCN (Figure 4d) to preserve information from different localities. TFGM-flavored weight-free GCN outputs the concatenation of normalized node embeddings from every layer. TFGM-flavored GCN performs better on differentiating blue nodes from purple nodes. In addition, TFGM-flavored GCN and weight-free GCN correctly reflect the symmetry positions of node pairs (4, 10) and (6, 5) in the network: two pairs of red nodes overlap in Figure 4d and Figure 4c.

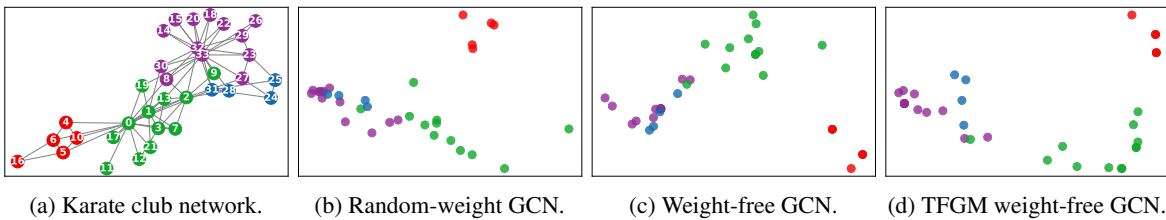


Figure 4: Visualization of the Karate club network’s node embedding from various training-free GCNs, all have 3 layers. Nodes of the same color are assigned to the same cluster (Blondel et al., 2008). We use PCA for 2-dimensional visualization. Figure 4d shows TFGM-flavored weight-free GCN.

Approximation of Random-weight GNNs. In Section 4.3, we present an interesting proposition that random-weight GNN approximates weight-free GNN for graph matching. To give empirical evidence, we show the performance difference between the weight-free and random-weight versions of the same GNN on DBP15k and PPI datasets (Table 8). We can see that 1) weight-free GNN consistently outperforms random-weight GNN; 2) the real performance reductions (0% ~ 2%) are negligible compared to the absolute values (30% ~ 80%). This verifies our claim that random-weight GNN is an unbiased estimator of weight-free GNN.

C.2 Experimental Setup

We implement all the models using PyTorch and PyTorch Geometric on a server with 500GB memory, two Intel CPU E5-2698 v4 (40 core), and an NVIDIA V100 GPU.

Table 8: The accuracy (%) reduction from random-weight GNNs to weight-free GNNs.

(a) DBP15k dataset.			(b) PPI dataset.										
	GraphSAGE	DGMC	Low-conf. Edges					Random Rewirement					
			Noise Ratio	5%	10%	15%	20%	25%	5%	10%	15%	20%	25%
ZH-EN	-0.3	-0.4	TFGM pos-enc										
JA-EN	-0.2	-0.2	GraphSAGE	-0.3	-0.3	-0.1	-0.0	-0.0	-0.7	-0.9	-1.1	-1.2	-0.1
FR-EN	-0.2	-0.1	DGMC	-1.0	-2.3	-0.8	-0.7	-0.8	-0.0	-0.7	-1.0	-1.5	-0.9

C.2.1 Baseline GNNs

We re-implement the GNNs following Algorithm 1 and remove the nonlinear activations between layers. In ablation studies (Section 5.4), we demonstrate that the nonlinear activation is not essential for TFGM’s performance. We also make necessary changes on architecture of baseline GNNs to adapt to the training-free setting.

GraphSAGE (Hamilton et al., 2017) usually achieves similar empirical performance with GCN but enjoys efficient deployment via neighbor sampling. Thus, we do not include GCN to avoid redundancy. We employ a weight-free sum aggregator, which is equivalent to the mean aggregator (Hamilton et al., 2017) because of the L_2 normalization in our implementation. We show in Table 8 that the weight-free version performs slightly better than the random-weight version.

SplineCNN (Fey et al., 2018; 2020) is a graph convolution kernel that can handle spatial geometric relation input. We use it to incorporate the spatial edge feature in natural images. Note that, SplineCNN has a complicated kernel function which is very different from our GNN definition (Section 3.1). Despite that, we show in experiments that TFGM can significantly improve its performance under the training-free setting. In TFGM, we keep SplineCNN’s randomly initialized weights unchanged. We also disable its residual connection.

DGMC (Fey et al., 2020) is the state-of-the-art GNN for graph matching. It iteratively refines the assignments and incorporates the inductive bias of neighborhood consensus (Rocco et al., 2018) that can preserve the edge compatibility between two graphs. DGMC uses another GNN as the backbone, which we switch between GraphSAGE or SplineCNN based on the dataset. In TFGM, we replace DGMC’s MLP for similarity measurement with training-free cosine similarity.

C.2.2 Datasets and Hyperparameters

Supervised Graph Matching. Keypoint matching is supervised graph matching to find the semantic equivalent keypoints between images of objects. We use the benchmark PascalVOC (Everingham et al., 2010) with Berkeley annotation (Bourdev and Malik, 2009). This dataset is fully supervised with the keypoint annotation for 20 categories of objects with at most 19 keypoints. For a fair comparison, our experimental setting is the same as (Fey et al., 2020). We use the pre-trained VGG16 (Simonyan and Zisserman, 2014) to obtain the initial node feature for keypoints. We use the train/test split from (Choy et al., 2016). We re-use the source code of (Fey et al., 2020) to pre-filter noisy images and keep images with at least one keypoint. We use the anisotropic edge feature due to the better performance. Following (Fey et al., 2020), we use argmax to obtain the approximate solution of the LAP. We use matching accuracy (%) as the evaluation metric. SplineCNN is only tested on PascalVOC because other datasets have no spatial edge features. For our models, the hidden dimension of GNNs is 512. Random dimension of DGMC is 128. GraphSAGE and SplineCNN have 5 layers. DGMC uses a 1-layer SplineCNN to perform the same number of refinements (20 steps) as in (Fey et al., 2020). The k -NN uses top 10 neighbors.

Semi-supervised Graph Matching. Entity alignment is a semi-supervised graph matching aiming to find equivalent entities between two heterogeneous KGs. We choose a popular benchmark DBP15k (Sun et al., 2017), involving three datasets between language pairs: Chinese to English (ZH-EN), Japanese to English (JA-EN), and French to English (FR-EN). Our experimental setup largely follows (Fey et al., 2020). We only use the entity names and graph structures in the dataset and do not use the relation types, attributes, and values. The node feature is initialized with the cross-lingual word embedding in (Xu et al., 2019). Following (Fey et al., 2020; Liu et al., 2021), we use argmax to obtain the approximate solution of the LAP. Following (Liu et al., 2021), we use Hit@1 (%), Hit@10 (%), and Mean Reciprocal Rank (MRR) as the evaluation metric. For our models, the hidden dimension of GNNs is 256. Random dimension of DGMC is 256. GraphSAGE has 2 layers. DGMC uses a 1-layer GraphSAGE to perform the same number of refinements (10 steps) as in (Fey et al., 2020).

Algorithm 1: TFGM (Unsupervised)

Input: $\{\mathcal{G}^{(s)}, \mathcal{G}^{(t)}\}$, GNN, $\{W_l\}_{l=1}^L$.
Output: S^* , U .

- 1 **for** \mathcal{G} in $\{\mathcal{G}^{(s)}, \mathcal{G}^{(t)}\}$ **do**
- 2 $(\mathcal{V}, A, X, E) \leftarrow \mathcal{G}$;
- 3 $H^{(0)} \leftarrow X$;
- 4 $F_i^{(0)} \leftarrow X_i / \|X_i\|_2, \forall i \in \mathcal{V}$;
- 5 **for** $l = 1 : L$ **do**
- 6 $F^{(l)} \leftarrow \text{GNN}(A, H^{(l-1)}, E, W_l)$;
- 7 $H^{(l)} \leftarrow \sigma(F^{(l)})$;
- 8 $F_i^{(l)} \leftarrow F_i^{(l)} / \|F_i^{(l)}\|_2, \forall i \in \mathcal{V}$;
- 9 **end**
- 10 $O \leftarrow [F^{(0)}; F^{(1)}; \dots; F^{(L)}]$;
- 11 **end**
- 12 $U_{ij} \leftarrow O_i^{(s)} \cdot O_j^{(t)}, \forall i \in \mathcal{V}^{(s)}, j \in \mathcal{V}^{(t)}$;
- 13 $S^* \leftarrow \operatorname{argmax}_{S \in \mathcal{T}} \sum_{i \in \mathcal{V}^{(s)}, j \in \mathcal{V}^{(t)}} S_{ij} U_{ij}$;

Algorithm 2: TFGMws for the supervised setting.

Input: $\{\mathcal{G}^{(s)}, \mathcal{G}^{(t)}\}$, $\mathcal{D} = \{\mathcal{G}^{(1)}, \dots, \mathcal{G}^{(N)}\}$, GNN, $\{W_l\}_1^L$.
Output: S^* , U .

- 1 **for** \mathcal{G} in $\{\mathcal{G}^{(s)}, \mathcal{G}^{(t)}\}$ **do**
- 2 $(\mathcal{V}, A, X, E) \leftarrow \mathcal{G}$;
- 3 **for** $\mathcal{G}^{(n)}$ in \mathcal{D} **do**
- 4 $\hat{S}^{(n)}, U^{(n)} \leftarrow \text{TFGM}(\{\mathcal{G}, \mathcal{G}^{(n)}\}, \text{GNN}, \{W_l\}_1^L)$;
- 5 **end**
- 6 **for** i in \mathcal{V} **do**
- 7 $\text{Scores} \leftarrow \{U_{iv}^{(n)} \mid \forall n \in [1, N], v \in \mathcal{V}^{(n)}, \hat{S}_{iv}^{(n)} = 1\}$;
- 8 $\mathcal{L} \leftarrow \{v \mid \forall U_{iv} \in \text{kLargest}(\text{Scores})\}$;
- 9 $\mathbf{k}_i \leftarrow \sum_{v \in \mathcal{L}} \mathbf{y}_v$; // \mathbf{y}_v is the one-hot encoding of node v 's label.
- 10 **end**
- 11 **end**
- 12 $U_{ij} \leftarrow \text{Cos}(\mathbf{k}_i^{(s)}, \mathbf{k}_j^{(t)}), \forall i \in \mathcal{V}^{(s)}, j \in \mathcal{V}^{(t)}$;
- 13 $S^* \leftarrow \operatorname{argmax}_{S \in \mathcal{T}} \sum_{i \in \mathcal{V}^{(s)}, j \in \mathcal{V}^{(t)}} S_{ij} U_{ij}$;

Unsupervised Graph Matching. Protein-Protein Interaction (PPI) Network Alignment is unsupervised and aims to find corresponding proteins in networks of different species (Elmsallati et al., 2015; Faisal et al., 2015). Following conventions (Saraph and Milenković, 2014; Vijayan et al., 2015), we use the high-confidence yeast *Saccharomyces cerevisiae* PPI network (Collins et al., 2007) as the source graph. The target graphs are generated by: 1) adding low-confidence edges into the source graph (Collins et al., 2007); 2) randomly rewiring the source graph (Saraph and Milenković, 2014). Each target graph has 5 versions of different noise ratios. For the Low-conf. Edges dataset, we report the average accuracy of 10 independent runs of TFGM. For the Random Rewirement dataset, we report the average accuracy of TFGM on the 10 synthetic datasets (Saraph and Milenković, 2014) at every noise ratio. Following (Zhang et al., 2019b), we solve the LAP using the Hungarian algorithm for TFGM and GHOST (Patro and Kingsford, 2012). For our models, the hidden dimension of GNNs is 512. GraphSAGE has 10 layers. DGMC uses a 1-layer GraphSAGE to perform 100 refinement steps. We compare with only training-free baselines because there is no supervision.

Algorithm 3: TFGMws for the semi-supervised setting.

Input: $\{\mathcal{G}^{(s)}, \mathcal{G}^{(t)}\}$, $\mathcal{I} = \{(i, j) | i \in \mathcal{V}^{(s)}, j \in \mathcal{V}^{(t)}\}$, GNN, $\{W_l\}_1^L$.
Output: S^* , U .

- 1 $(\mathcal{V}^{(s)}, A^{(s)}, X^{(s)}, E^{(s)}) \leftarrow \mathcal{G}^{(s)}$;
- 2 $(\mathcal{V}^{(t)}, A^{(t)}, X^{(t)}, E^{(t)}) \leftarrow \mathcal{G}^{(t)}$;
- 3 $\hat{X}^{(s)} \leftarrow X^{(s)}$; $\hat{X}_i^{(s)} \leftarrow X_j^{(t)}, \forall (i, j) \in \mathcal{I}$;
- 4 $\hat{X}^{(t)} \leftarrow X^{(t)}$; $\hat{X}_j^{(t)} \leftarrow X_i^{(s)}, \forall (i, j) \in \mathcal{I}$;
- 5 $\hat{\mathcal{G}}^{(s)} \leftarrow (\mathcal{V}^{(s)}, A^{(s)}, \hat{X}^{(s)}, E^{(s)})$;
- 6 $\hat{\mathcal{G}}^{(t)} \leftarrow (\mathcal{V}^{(t)}, A^{(t)}, \hat{X}^{(t)}, E^{(t)})$;
- 7 $-, U^{(s)} \leftarrow \text{TFGM}(\{\hat{\mathcal{G}}^{(s)}, \mathcal{G}^{(t)}\}, \text{GNN}, \{W_l\}_1^L)$;
- 8 $-, U^{(t)} \leftarrow \text{TFGM}(\{\mathcal{G}^{(s)}, \hat{\mathcal{G}}^{(t)}\}, \text{GNN}, \{W_l\}_1^L)$;
- 9 $U \leftarrow U^{(s)} + U^{(t)}$;
- 10 $S^* \leftarrow \operatorname{argmax}_{S \in \mathcal{T}} \sum_{i \in \mathcal{V}^{(s)}, j \in \mathcal{V}^{(t)}} S_{ij} U_{ij}$;

D Algorithms

We present the pseudocode of the unsupervised TFGM and the supervised and semi-supervised versions of TFGMws algorithms. Both the supervised and semi-supervised TFGMws rely on the unsupervised TFGM. For all settings, we aim to find the assignment matrix S^* between two input graphs $\mathcal{G}^{(s)}$ and $\mathcal{G}^{(t)}$.

Unsupervised TFGM. Following Algorithm 1, we can obtain the assignment matrix S^* by solving the LAP. The similarity matrix U is used in supervised and semi-supervised TFGMws to account for annotation. We use a generalized GNN(A, X, E, W) which can utilize edge features E . The weight W can be discarded if using weight-free GNNs.

First, we normalize each node’s feature vector. Then, for each layer GNN, their outputs are (optionally) fed into a nonlinear activation function to be used as inputs in the next layer. After that, we normalize the GNN outputs to ensure equal importance for the comparison of different localities. Finally, we concatenate the GNN outputs from all layers as the final node embeddings. Thus, the dot product in Line 12 is equivalent to the summation of cosine similarity in Equation (5). We use an off-the-shelf LAP solver, *e.g.*, Hungarian or argmax , to solve the LAP. We use the same LAP solver as the baselines in experiments for fair comparison.

Supervised TFGMws. In keypoint matching of natural images, the training dataset $\mathcal{D} = \{\mathcal{G}^{(1)}, \mathcal{G}^{(2)}, \dots\}$ contains graphs of the same object, *e.g.*, motorbike. Algorithm 2 present the steps for the supervised TFGMws. The algorithm has two phases: 1) generating \mathbf{k}_i and 2) solving the LAP for S^* with node similarity measured by $\operatorname{Cos}(\mathbf{k}_i^{(s)}, \mathbf{k}_j^{(t)})$, $\forall i \in \mathcal{V}^{(s)}, j \in \mathcal{V}^{(t)}$. To generate \mathbf{k}_i from \mathcal{G} , we first conduct graph matching between \mathcal{G} and every graph in \mathcal{D} . TFGM returns matrix $U^{(n)} \in \mathbb{R}^{|\mathcal{V}| \times |\mathcal{V}^{(n)}|}$, which measures the similarity scores between nodes in \mathcal{G} and $\mathcal{G}^{(n)}$. Next, for every $\mathcal{G}^{(n)} \in \mathcal{D}$, we select the node that is equivalent to i (based on $\hat{S}^{(n)}$), giving us totally N nodes. Finally, we keep the k nodes with the largest similarity to i and use the sum of the one-hot encoding of these k nodes as \mathbf{i} .

Semi-supervised TFGMws. In Algorithm 3, we utilize the annotation in semi-supervised graph matching by forcing the known equivalent node pairs to have the same initial feature. Note that, we conduct TFGM twice by comparing $\hat{\mathcal{G}}^{(s)}$ with $\mathcal{G}^{(t)}$ and comparing $\mathcal{G}^{(s)}$ with $\hat{\mathcal{G}}^{(t)}$. Further, we ensemble the two node similarity matrices $U^{(s)}$ and $U^{(t)}$ to achieve better performance.